Available online at www.sciencedirect.com
SCIENCE DIRECT®
International Journal of Heat and Mass Transfer 49 (2006) 3583–3594
International Journal of HEAT and MASS TRANSFER
www.elsevier.com/locate/ijhmt

Interface conditions governing evaporation of stored liquids in presence of non-condensable gas

K. Ramamurthi [a,*], S. Sunil Kumar [b], B.S. Chaitanya [c]

[a] Department of Mechanical Engineering, Indian Institute of Technology Madras, Chennai 600 036, India
[b] Liquid Propulsion Systems Centre, Trivandrum 695 547, India
[c] ISRO Satellite Centre, Bangalore 560 017, India

Received 24 June 2005
Available online 21 April 2006

Abstract

Experiments were conducted to determine the variation of interface temperatures during the storage and draining of liquid nitrogen from large containers in the presence of the non-condensable gas. A chilled layer was seen to be formed at the interface in the presence of the non-condensable gas and this layer advanced into the warm liquid at speeds higher than the characteristic speeds associated with thermal diffusion. A theoretical model was developed for the interface temperatures considering the evaporation from the stratified layer in the stored column of liquid. The predictions of the model were shown to compare well with the experimental measurements. A correlation was obtained for the interface temperatures when the proportion of the non-condensable gas was varied.

Keywords: Interface; Saturation temperature; Non-condensable gases; Stratification

1. Introduction

Evaporation from a liquid surface depends on the temperature of the liquid–vapor interface, the fractional concentration of the evaporating liquid present in the gas phase at the interface, the temperature of the gas phase and the area of the liquid–vapor interface. The kinetic model of evaporation considers vaporization to be driven by the excess partial pressure of the vapor of the evaporating liquid. The hydrodynamic model considers the diffusion of the vapor of the liquid away from the liquid vapor interface. The vapor pressure at the interface is assumed to be saturated corresponding to the liquid surface temperature. Kryukov et al. [1] show that the overall trends for the evaporation of diesel fuel obtained from kinetic and hydrodynamic models are about the same at different ambient pressures. However, at lower values of ambient pressure the values of evaporation rate predicted by the hydrodynamic model are generally higher than by the kinetic model. Kozyrev and Sitnikov [2] demarcate two regions of evaporation as the regime of diffusion and depletion. Irrespective of whether kinetic or hydrodynamic models are used, it is necessary to specify the conditions at the interface for predicting the evaporation. The present investigation deals with experimental measurements of the temperature at interfaces of liquids stored in containers.

The presence of non-condensable gases at liquid–vapor interfaces provides resistance to the evaporation. Scurlock [3] suggests that the surface temperature of an evaporating liquid should be significantly higher when a nano-layer of insoluble molecules builds up on the surface. In many applications involving evaporation of liquids stored in containers, non-condensable gases are invariably present above the liquid–vapor interfaces. Any prediction methodology for the convective motion in the stored liquid or the formation of a stratified layer or evaporation and condensation at the surface would require the input of surface temperature or the partial pressure of the vaporizing

* Corresponding author. Tel.: +91 44 225 74704; fax: +91 44 225 70509.
E-mail address: krmurthi@iitm.ac.in (K. Ramamurthi).

0017-9310/$ - see front matter © 2006 Elsevier Ltd. All rights reserved.
doi:10.1016/j.ijheatmasstransfer.2006.02.041

Nomenclature

a	binary-contact area per unit volume (m^{-1})
C_P	specific heat at constant pressure ($J\,kg^{-1}\,K^{-1}$)
D_{A-B}	binary diffusivity of component A in B ($m^2\,s^{-1}$)
h	heat transfer coefficient without mass transfer ($W\,m^{-2}\,K^{-1}$)
i_{l-g}	heat of vaporization ($J\,kg^{-1}$)
i	specific enthalpy ($J\,kg^{-1}$)
κ	mass transfer coefficient without mass transfer ($kg\,m^{-2}\,s^{-1}$)
Nu	Nusselt number
P	total pressure (Pa)
p	partial pressure (Pa)
q	heat transfer rate per unit volume ($W\,m^{-3}$)
Pr	Prandtl number
Ra	Raleigh number
Re	Reynolds number
Sc	Schmidt number
Sh	Sherwood number
T	temperature (K)
W	molecular weight ($kg\,mol^{-1}$)
x	mole fraction
y	coordinate normal to interface (m)
α	thermal diffusivity ($m^2\,s^{-1}$)
Γ	mass transfer rate at the interface per unit volume ($kg\,s^{-1}\,m^{-3}$)
k	thermal conductivity ($W\,m^{-1}\,K^{-1}$)
ρ	density ($kg\,m^{-3}$)
ω	mass fraction

Subscripts

g	vapor mixture
i	interface
nc	non-condensable gases far away from the interface
o	condensation site
sat	saturation
∞	bulk
v	condensable vapor
s	interface
c	critical

Superscript

*	coefficient with mass transfer

liquid at the interface and these are influenced by the presence of the non-condensable gases.

Gerner and Tien [4] developed a model for interfacial heat and mass transfer for a circulating liquid pool when non-condensable gases are present. The temperature and mass fraction of the non-condensable gases were determined in the model as a function of the distance from the interface. At the interface, the fraction of the non-condensable gases and the saturation temperature were related to the total pressure assuming local equilibrium and the saturation curve was assumed to obey the Clausius–Clapeyron equation.

Krahl and Adamo [5] more recently developed the governing equations for a two phase flowing system in presence of vaporization when non-condensable gases were present. Morita et al. [6] developed a generalized model for multiphase flow with heat transfer and diffusion at the interface. Moggin et al. [7] carried out detailed computations of the motion of liquid surface in tanks from buoyancy and Marangoni convection in which the concentration of non-condensable gases was also incorporated.

The early work of Clark [8] considers the solution of one-dimensional heat conduction and diffusion equations for defining the interface temperature and concentration in the presence of non-condensable gases. Condensation was found to be greatly reduced by using a non-condensable helium gas over a stored volume of liquid oxygen.

Though a large body of literature exists on computational and phenomenological models, an 'a priori' procedure for readily estimating the role of non-condensable gas in modifying interface conditions is not available. A change in the interface conditions would have significant influence not only on the rate of evaporation but also on the convection currents and the extent of build-up of stratified layer and hence on the venting and pressurization requirements. The instabilities and explosions of dewars containing cryogens [3] could be traced to the interface. The recent work of Fedorov and Luk'yanova [9] on the storage of liquid hydrogen at ambient pressure in insulated containers discusses the formation of cooler interface at the top of a warmed-up stratified column of liquid hydrogen in the presence of a non-condensable helium gas. This would lead to a fall in the evaporation.

The precise temperature measurements of Fang and Ward [10] at the liquid vapor interface when a liquid viz., water was surrounded by its vapor showed the temperature of vapor at the interface to be greater than the temperature of the liquid at the interface. The difference in the two temperatures was also shown to increase as the rate of evaporation increased. Higher values of vapor temperature are not consistent with the generalized notion of superheat in the liquid being required to drive the evaporation. Beduz et al. [11] suggested that surface of liquid oxygen and liquid nitrogen should be superheated by about 4 K for evaporation to take place. Clark [8] gives the surface temperatures to be negligibly different from the saturated value except at "vanishingly" small times. Large values of liquid superheat are associated with fast or flash evaporation. Peterson et al. [12] show fast evaporation and flashing to be caused by

severe convective motion and entrainment of droplets of cold liquid with the vapor during the vaporization. Gemci et al. [13] use the flashing process to determine the atomization at different temperatures and pressures.

A series of experiments is conducted in the present investigation with liquid nitrogen (LN_2) stored in large insulated tanks to determine the interface conditions in the presence of a non-condensable gas. Predictions are thereafter done for a stratified column of liquid and the theoretical predictions are compared with the results from experiments. The influence of the rate of evaporation is separately studied in small containers with distilled water using sub-atmospheric pressures to drive the vaporization. Sections 2 and 3 give the details of the experiments and results obtained. Section 4 deals with the theoretical predictions. The conclusions are summarized in Section 5.

2. Experiments

Two types of experiments were carried out on the liquid–vapor interfaces. In the first set of experiments, a 0.25 m^3 foam-insulated tank of diameter 0.6 m and height of 1.4 m was filled with liquid nitrogen (LN_2) and drained at two different values of pressure using gaseous helium. The temperature in the gas, interface and bulk liquid were measured during the draining. The second set of experiments was on evaporation of distilled water in a rectangular glass chamber of $0.03\ m \times 0.03\ m \times 0.007\ m$. The evaporation was carried at sub-atmospheric pressures. The density gradient at the water/vapor interface and the convection currents were observed in this small chamber using a schlieren set-up. The temperatures in the liquid, interface and vapor were also measured.

2.1. Experiments in 0.25 m^3 LN_2 container pressurized with gaseous helium

A schematic of the set-up and the measurements are shown in Fig. 1. Temperatures were measured at 18 axial locations and four radial locations using platinum resistance thermometers (RTD). The RTDs were placed 1 cm apart on a Teflon rod of 0.02 m diameter and the rod was centered along the axis of the tank. The RTDs were connected to a 30 channel mobile data recorder with provision to scan all the temperature sensors in one second interval. The measurement accuracy was ±0.15% and the resolution in temperature was 1 K.

The tank was provided with vent, pressurization and relief valves as shown. It was filled with LN_2 at a temperature of 80 K after initially chilling the tank with cold nitrogen vapor. The fill line was connected to a large LN_2 storage tank of about 10 m^3 capacity at 0.35 MPa through a 10 m long stainless steel pipe of 0.017 m diameter. The level of LN_2 in the tank was monitored using a capacitance type level sensor mounted along with the central Teflon instrumentation rod. The level of liquid nitrogen in the

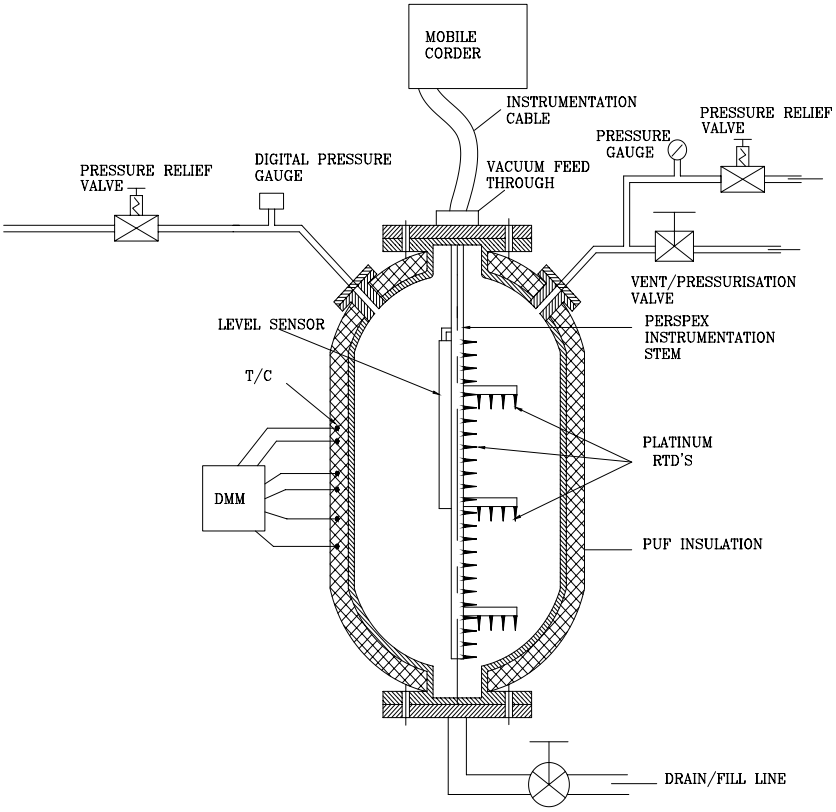

Fig. 1. Experimental set-up of LN_2.

tank was also determined at the different instants of time from a digital weighing balance with a platform of 1 m × 1 m on which the tank rested. The measurement range was 1000 kg with a resolution of 0.05 kg and an accuracy of ±0.01% of the full scale.

The tank was heated circumferentially using four infrared lamps positioned at the mid-length of the tank to accelerate the heat-in-leak and aid the formation of a stratified layer. The ullage was then pressurized with helium gas to a pressure of 0.20 and 0.25 MPa, respectively. When steady temperature conditions were reached in the ullage gas, with the column of LN_2 comprising of a stratified layer over the bulk sub-cooled liquid (schematically shown in Fig. 2), regulated draining was started keeping the ullage gas pressure constant. Topping of the ullage gas was done by admitting gaseous helium at a temperature of 100 K into the ullage in the different sets of experiments. This gave increasing values of helium concentration in the ullage gas. The ullage pressure was controlled within ±0.01 MPa, the measurement of pressure being done by a digital manometer with an accuracy of ±0.05%.

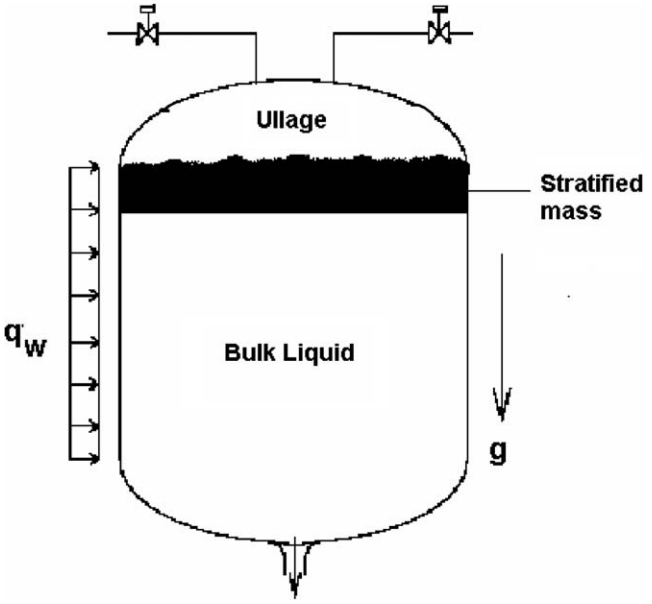

Fig. 2. Schematic of evaporation from stratified layer.

The temperature along the length of the LN_2 column was measured as the draining progressed. The temperature history was obtained by five representative sensors (1–5) mounted at five different heights of the liquid column as illustrated in Fig. 3. The pressure was maintained at 0.25 MPa and the average draining rate was 0.32 kg s^{-1}. The interface of the liquid is exposed to helium and vapor. Surface temperatures were not seen to correspond to the saturation temperature corresponding to the ullage pressure. As the fluid is drained, each of the sensors measured the interface temperature based on its respective position. It is to be noted here that the pressurization with helium gas was initiated only after a stratified layer of liquid was formed at the surface. The temperature increased from the bulk to the stratified region (shown by AB) and thereafter gradually decreased reaching a lowest value at the interface represented by 'C' before getting exposed to the gas. That this lowest temperature corresponded to the interface was checked with respect to the height of the liquid available in the tank, from the level sensor measurements and counter checked with the weight measurements of the tank. The subsequent increase in temperature after C in Fig. 3 indicates that the sensor is in the vapor column.

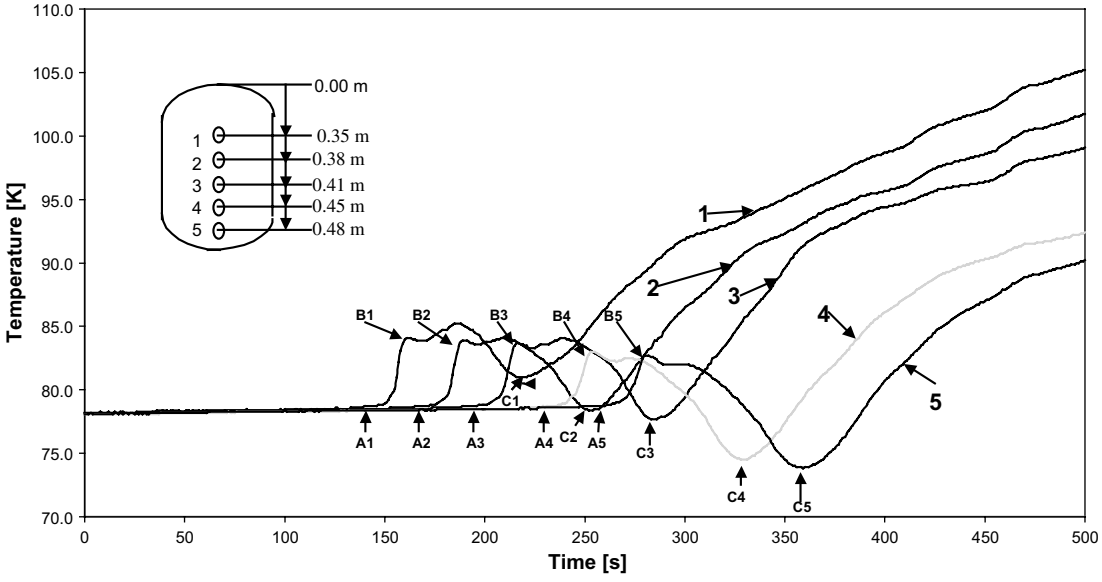

Fig. 3. Variation of temperature with time at different location in LN_2.

There is no discrete change or discontinuity in the temperature at the interface and is demonstrated by the continuity of the measured values of temperature at C.

The existence of a cooler interface above the hot sub-layer is seen in all axial temperature measurements of which five are shown in Fig. 3. Similar trends were also obtained with ullage gas pressure of 0.20 MPa with a draining rate of 0.20 kg s^{-1}. It is seen from Fig. 3 that the hot sub-layer cools down with time (B5 < B4 < B3 < B2 < B1), and the interface temperature also decreases (C5 < C4 < C3 < C2 < C1). The extent of this cooler interface region, wherein the temperature is below the warm stratified layer, grows with time as draining progress. This corresponds to the time between B and C in Fig. 3.

The ullage volume in these experiments was pressurized with helium, leading to a progressive fall in the partial pressure of nitrogen as the draining continued. The decreased partial pressure is responsible for the reduction in liquid surface temperature as seen from the temperatures C1–C5 in Fig. 3.

2.2. Experiments in the small chamber with water

Fig. 4 is a schematic of the experimental set-up of the $0.03 \times 0.03\ \text{m} \times 0.007\ \text{m}$ chamber containing water. The pressure of the vapor above the interface was varied between 5×10^{-4} and 40×10^{-4} MPa by connecting the chamber to a rotary vacuum pump using a low pressure line regulator and a flow control valve. The thermocouples were mounted at different locations inside the chamber to measure ullage, bulk and interface temperatures apart from the wall temperatures. The thermocouples were connected to a mobile recorder as in the previous experiments. The measurement accuracy was within ±0.2%. The vacuum pressures were measured using a Pirani gauge with accuracy better than ±20%.

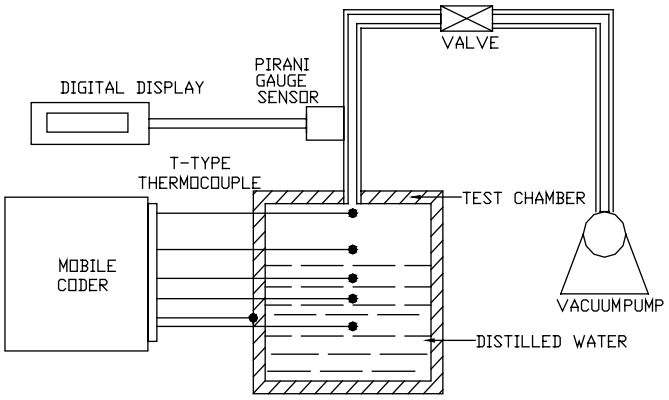

Fig. 4. Schematic of experiments with water.

The chamber was partly filled with distilled water so that some of the thermocouples would be in the liquid and a few in the vapor region. The vacuum pump was activated and the line pressure regulator and valve were adjusted so that the non-condensable gases and the trapped gas in the water are removed under low vacuum (10^{-2} MPa). Subsequently, the valve was fully opened and the desired vacuum level attained in the ullage using the line pressure regulator.

A typical trace of variation of temperatures in the liquid and gas with time is shown in Fig. 5 when the ullage gas pressure was kept at a low value of 9×10^{-4} MPa. Irregular time dependent variation with periodic spikes is observed in all the measured temperatures. Scurlock [3] has observed such irregular temperature variations and attributed them to turbulent convection cells. Flow visualization using schlieren showed the formation of bubbles near the interface and convective motion of the bubbles followed by

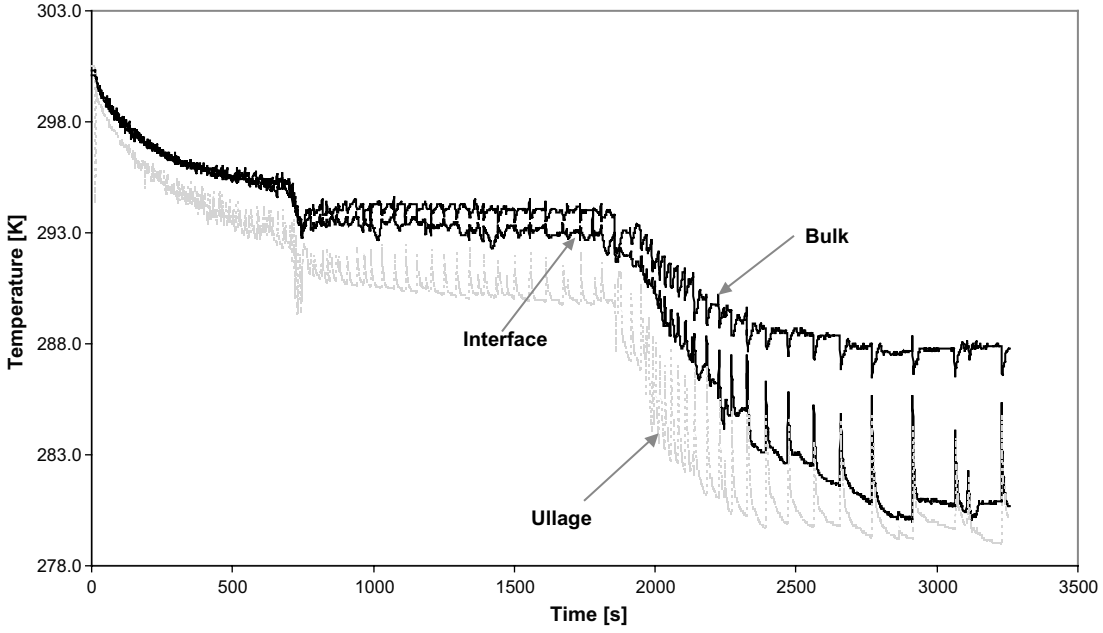

Fig. 5. Disruptive evaporation with water.

violent explosion of the bubble below the interface. It seems likely that the violent collapse of the bubble leads to the thermocouple periodically seeing the vapor instead of the liquid and vice versa and this could be the cause of the irregular time dependent variations.

In the experiments with large tanks, the buoyancy forces are important and give rise to convection. This is not present in the small volume containing water. The localized nature of burst of bubbles and the local vaporization could lead to horizontal temperature gradients and surface tension induced currents.

3. Analysis of experimental results

3.1. Interface temperatures

The measured values of the interface temperatures for LN_2 in presence of helium gas at pressures of 0.25 and 0.20 MPa are shown in Fig. 6 as a function of the fraction of the non-condensable helium in the ullage gas. It is seen that as the non-condensable helium fraction increases, the surface temperature drops due to the lower concentration of the pure vapor at the interface. As ullage pressure

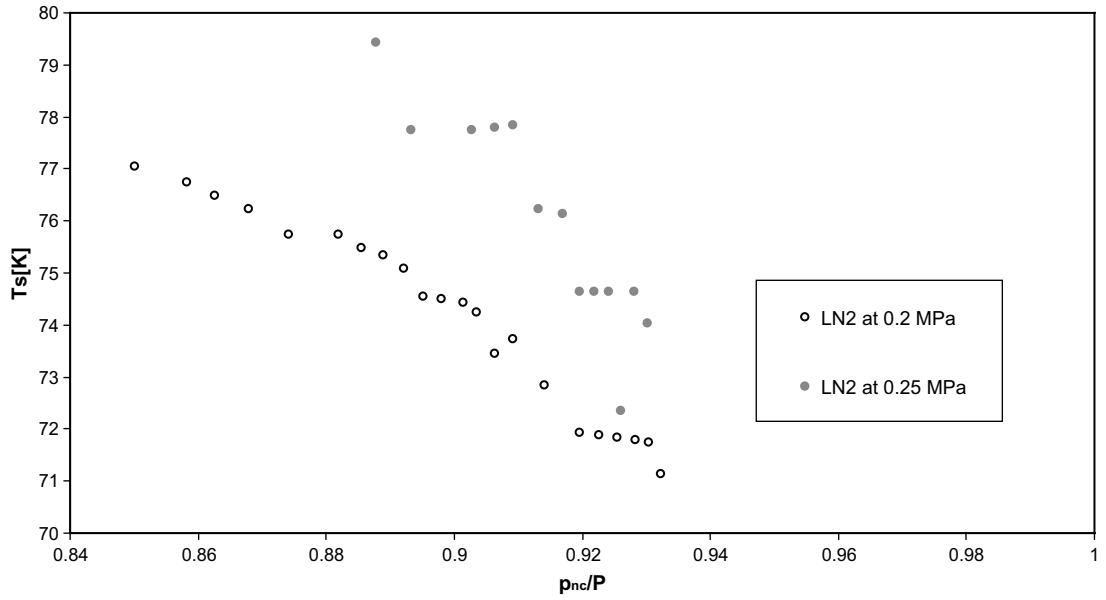

Fig. 6. Variation of surface temperature in different experiments.

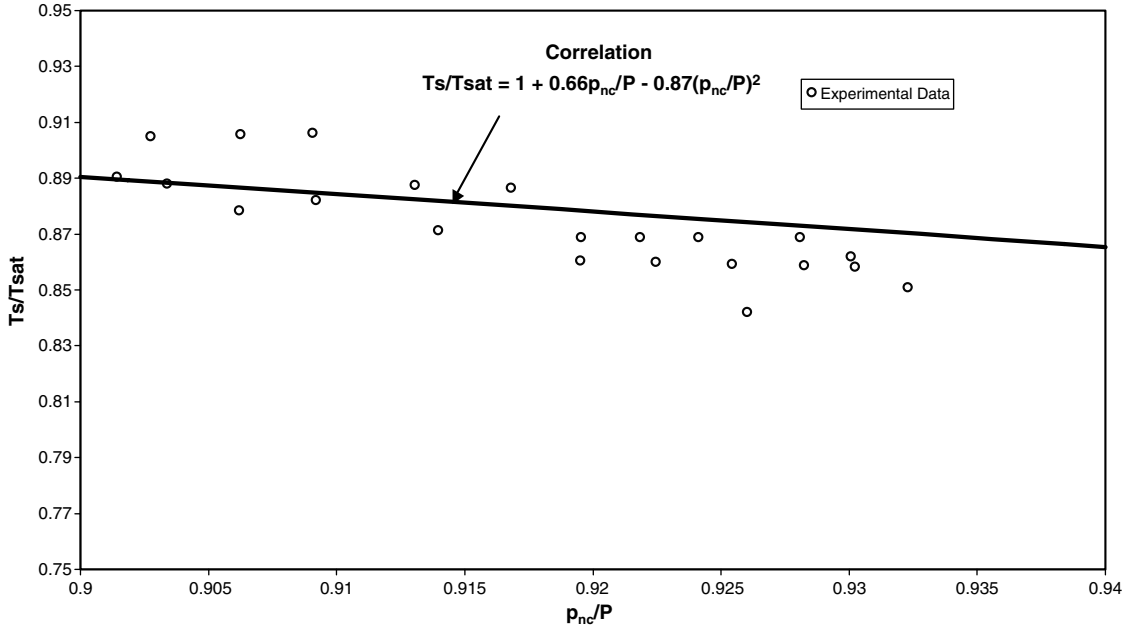

Fig. 7. Variation of non-dimensionlised surface temperature in different experiments.

increases from 0.2 to 0.25 MPa, the interface temperature increases for a given fraction of the non-condensable gases. The higher interface temperature could be from the higher energy transfer to the interface from the ullage gas and a larger proportion of the pure vapor at the interface.

When the measured values of surface temperatures were non-dimensionlised by the saturation temperature corresponding to the total pressure and plotted as a function of the fraction of non-condensable, a plot as shown in Fig. 7 is obtained. The non-dimensionlised interface temperature falls as the fraction of the non-condensable gas is increased. All 28 data points of LN_2, for values of ullage pressure between 0.20 and 0.25 MPa over which experiments were conducted, fall reasonably well on a second degree curve. The second degree was selected based on the trend given by the model predictions, discussed subsequently. When no condensable gas is present, the non-dimensional surface temperature is unity. A curve fit of the experimental data gives the relation:

$$\frac{T_s}{T_{sat}} = 1.0 + 0.66\frac{p_{nc}}{P} - 0.87\left(\frac{p_{nc}}{P}\right)^2 \quad (1)$$

where p_{nc} is partial pressure of the non-condensable gas far away from the interface and P is the total pressure. The validity of this correlation is for values of p_{nc}/P between 0.9 and 0.94 over which the experiments were conducted.

During the experiment, the ullage pressure was maintained constant. The amount of pressurant required for maintaining constant ullage pressure is estimated based on the outflow mass flow rate of the liquid and initial ullage volume. Using this additional pressurant mass and initial mass fraction of the non-condensable gas before pressurization, the partial pressure of the non-condensable gases (p_{nc}) is estimated.

3.2. Interface pressures

The surface temperature at the interface driving the evaporation is the saturation temperature corresponding to the partial pressure of the vapor of the evaporating liquid at the interface. The partial pressure of the vapor at the interface would increase as the ullage pressure increases and decrease as the fraction of non-condensable gas increases. Denoting the interface pressure of vapor as $p_{v,i}$ and the partial pressure of the vapor and the non-condensable gases in the ullage as $p_{v,\infty}$ an p_{nc}, respectively, a relationship between $p_{v,i}$, $p_{v,\infty}$ an p_{nc} of the following form could be assumed:

$$p_{v,i} = p_{v,\infty} + xp_{nc} \quad (2)$$

Here, x denotes the correction factor for the pressure of the vapor at the interface due to the influence of the non-condensable gases. If the surface temperature data obtained in all the experiments involving LN_2 are put together and the value of $p_{v,i}$ is taken as the saturation pressure at the surface temperature T_s (determined using ALLPROPS [17]), the variation of x in above equation with changes in the fraction of non-condensable gases can be determined. The value of p_{nc} and $p_{v,\infty}$ are determined from the total pressure depending on the quantity of non-condensable helium added to the ullage. Fig. 8 gives the variation of x as a function of the fraction of the non-condensable gases. A regression fit of the data gave a correlation

$$x = 2512.6e^{-10.2\frac{p_{nc}}{P}} \quad (3)$$

Here, P is the total pressure in the ullage volume. As the partial pressure of the non-condensable gases increases, the factor enhancing the interface vapor pressure decreases. When non-condensable gases are not present, the partial

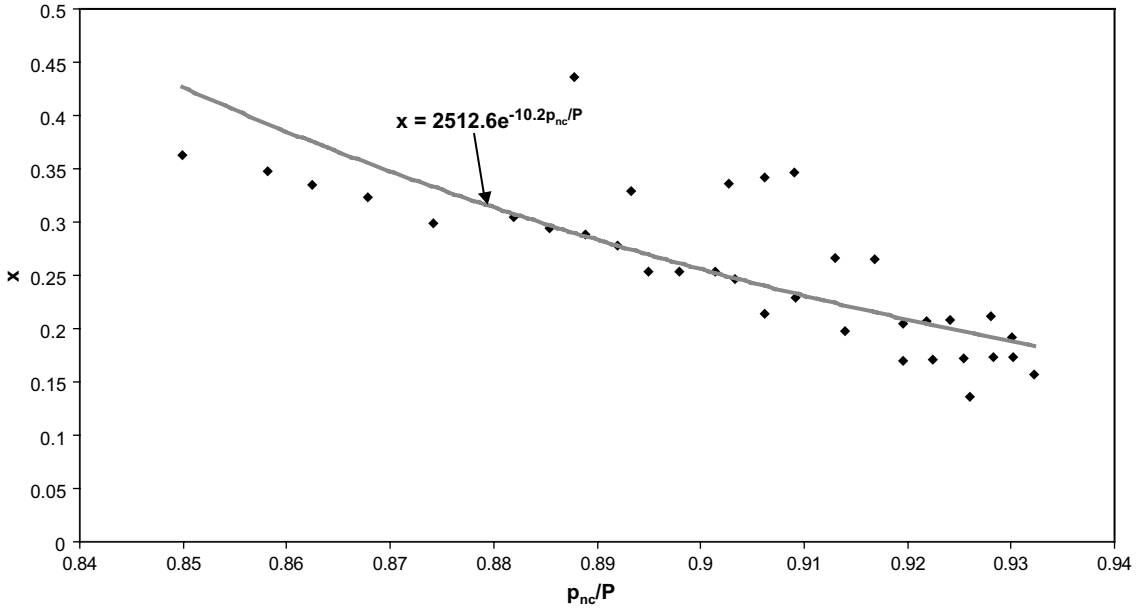

Fig. 8. Correlation of partial pressure of vapor at interface.

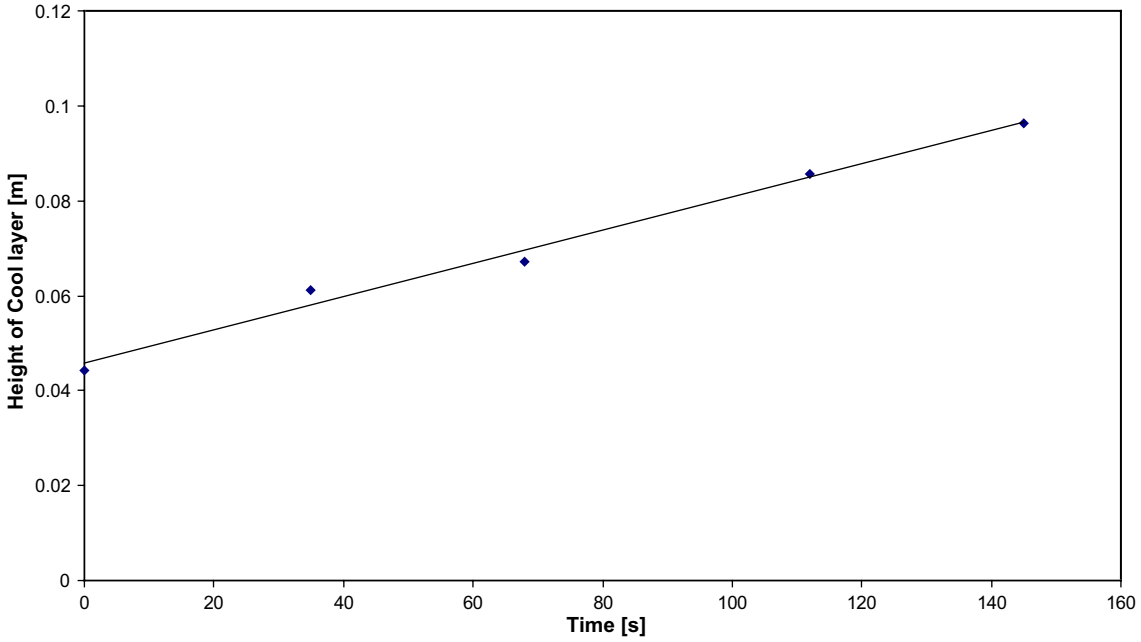

Fig. 9. Growth of chill layer in LN_2.

pressure of the pure vapor at the interface and the far field are the same.

3.3. Propagation of cold interface in the superheated liquid

The measured value of temperature at the liquid interface was seen to be lower than the temperature of the stratified layer of LN_2 in Fig. 3. The interface temperature was seen to progressively decrease as helium concentration in the ullage increased. The cooler surface was also seen to penetrate into the warmer liquid. The growth of the chill layer with time is shown in Fig. 9 for LN_2. Here, the chill layer corresponds to the region wherein the minimum surface temperature diffuses into the warmer liquid. It is determined as the product of time between events B and C (Fig. 3) and the rate at which surface of the liquid regresses during the depletion. Over a period of 140 s, the growth of the chill layer in LN_2 is 40 mm. The rate of growth is about 0.3 mm s^{-1}. If the growth of the chill surface layer is by thermal diffusion alone, the extent should be of the order of $\sqrt{\alpha t}$ giving a growth rate of 3.3 mm for liquid nitrogen. This is a gross underestimate by more than an order of magnitude. The thermal diffusion at these low temperatures and the influence of stratification currents on propagation of the chill layer need to be investigated further.

3.4. Variations in interface temperatures

The experiments on evaporation of water at different saturation pressures showed the intensity of bubble formation and bursting to decrease as the ullage pressure increased from 9×10^{-4} to 80×10^{-4} MPa. A plot of the ullage and interface temperatures with changes in the ratio of ullage pressure is given in Fig. 10. The saturation temperature, calculated from the ullage pressure, is shown by the dotted line. The ullage pressure is non-dimensionlised with respect to the saturation pressure corresponding to the bulk temperature of the liquid. It is seen that the interface temperature is significantly different from the saturation temperature at lower values of ullage pressure. At these pressures, there is a strong convective current in the liquid resulting in disruptive evaporation, leading to mixing

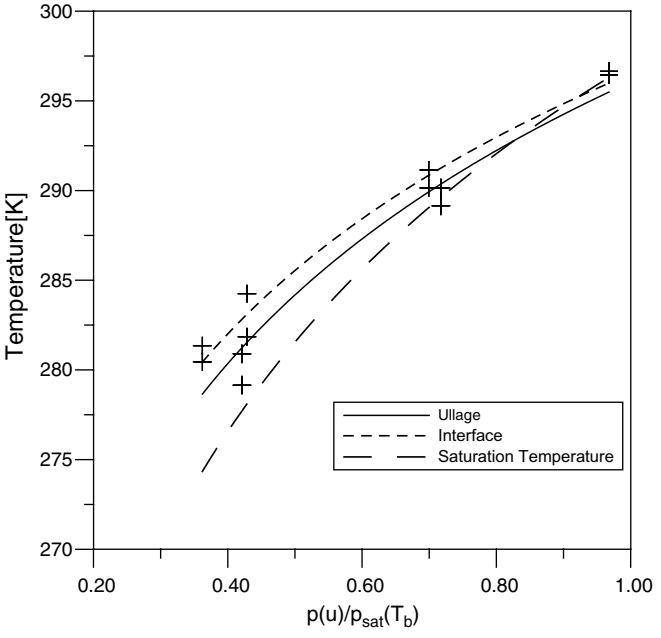

Fig. 10. Variation in interface, ullage and saturation temperature with change in ullage pressure.

of the warmer bulk liquid with the cooler interface. This raises the surface temperature above the saturation value. As the ratio of ullage pressure to the vapor pressure corresponding to the bulk temperature of liquid increases, the disruptive evaporation decreases, bringing the two temperatures closer. When the ratio is higher than 0.8, evaporation without significant disruption of the surface occurs and the interface, ullage and saturation temperature are about the same. The results indicate that under fast disruptive evaporation, interface temperature can be significantly different from the saturation temperature.

4. Predictions

Predictions for the interface conditions were carried out by extending the model of Morita et al. [6] developed for a flowing multiphase/multicomponent system to evaporation of a stratified mass of stored liquid. The model considers the diffusion of heat and mass from the surface in presence of a non-condensable gas [14]. A schematic of the model is shown in Fig. 11. The interface is shown by I and a stratified liquid region extends over a thickness Δ as shown. In the vapor region, a mixture of pure vapor at partial pressure p_v and non-condensable gas at partial pressure p_{nc} is considered. ω_∞ is the mass fraction of the pure vapor in the mixture. The mass fraction of vapor continuously increases from ω_∞ to ω_i towards the interface as shown in Fig. 11. The diffusion of vapor from the evaporating surface is determined in the model by mass and energy balance and is discussed below.

Assuming that mass diffusion due to thermal and pressure gradient is negligibly small, the mass transfer rate of vapor component (Γ) per unit volume at the interface I is defined to be negative for evaporation and is governed by the diffusion equation given by Bird et al. [15]

$$\Gamma = a_i \rho_g D_{v\text{–}nc} \left.\frac{d\omega}{dy}\right|_i + \omega_i \Gamma \tag{4}$$

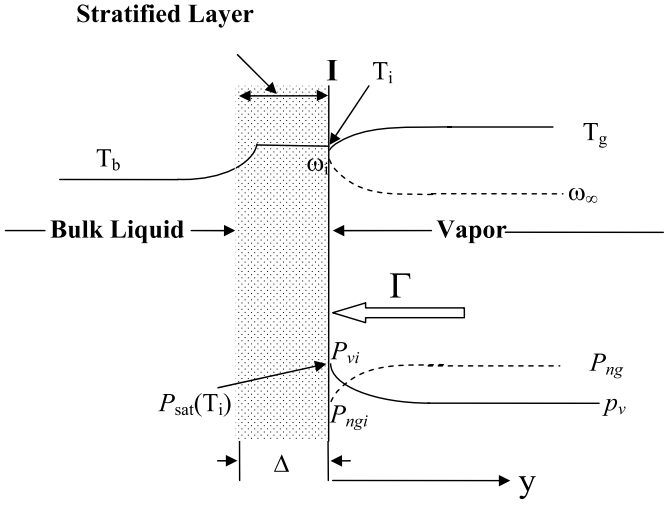

Fig. 11. Schematic of model.

where a_i is the binary-contact area per unit volume and subscript 'i' refers to the location at the interface. ρ_g and $D_{v\text{–}nc}$ are density and mass diffusivity of the vapor mixture, respectively. ω is the mass fraction of the vapor. Coordinate y refers to the normal to the interface as shown in Fig. 11. $\left.\frac{d\omega}{dy}\right|_i$ is the gradient of mass fraction of the vapor in the y direction at the interface.

The right side of the above equation includes both the diffusive and convective contributions. The mass diffusion from thermal and pressure gradients is neglected.

The heat transfer at the interface (q_i) is formulated by taking into account the contribution of heat conduction, and diffusion. Approximating the temperature gradients by overall heat transfer coefficients, the energy balance yields

$$a_i h_g^*(T_i - T_g) - \Gamma i_g = -k a_i \left.\frac{dT}{dy}\right|_i - \Gamma i_0 \tag{5}$$

where h_g^* is the vapor side heat transfer coefficient in presence of mass transfer and i_g and i_0 are specific enthalpy of saturated vapor and liquid, respectively. This equation implies that the heat flow at the interface equals the sum of the latent heat and the sensible heat. The conduction term $k\left.\frac{dT}{dy}\right|_i$ at the interface is zero, since a stratified liquid is considered. The constant temperature in the liquid is justifiable for problems involving stored liquids since the top region comprises of the stratified warm liquid. The surface of the liquid–vapor interface is assumed to be planar though in practice the surface tension forces would cause the surface to be curved. Ripples at the interfaces are neglected.

Eq. (4) is simplified by introducing the mass transfer coefficient in a manner analogous to the heat transfer coefficient, that is

$$\rho_g D_{v\text{–}nc} \left.\frac{d\omega}{dy}\right|_i = -\kappa^*(\omega_i - \omega_\infty) \tag{6}$$

where κ^* is the mass transfer coefficient. Eqs. (4) and (5) after simplification can be combined into the following single algebraic equation:

$$\kappa^*(\omega_i - \omega_\infty) i_{l\text{–}g} + \omega_i i_{l\text{–}g}(\kappa^*(\omega_i - \omega_\infty))/\omega_{nc} = -(h_g^*(T_i - T_g)) \tag{7}$$

where $i_{l\text{–}g}$ is the latent heat of vaporization and corresponds to the enthalpy difference between i_g and i_0.

The mass fraction ω_i of the vapor component at the interface is determined from the mole fractions (x):

$$\omega_i = x_i W / (x_i W + x_{nc} W_{nc}) \tag{8}$$

where W and W_{nc} are molecular weight of vapor and non-condensable gas, respectively. The mole fraction of vapor component at the interface is obtained by assuming a constant pressure in the gas boundary layer at the interface. Treating the vapor component and non-condensable gases as a mixture of ideal gases, the mole fraction x_i of vapor component at the interface is related to the interface temperature T_i according to

$$x_i = \frac{p_{sat}(T_i)}{P} \tag{9}$$

Here, $p_{sat}(T_i)$ is the saturation pressure of a vapor component at the interface and P is the total pressure.

The total pressure P at the interface is expressed as the sum of $p_{sat}(T_i)$ and the partial pressure of the non-condensable gases at the interface $p_{nc,i}$

$$P = p_{sat}(T_i) + p_{nc,i} \tag{10}$$

The interface temperature is obtained iteratively by solving Eqs. (7)–(10) simultaneously using Newton Raphson method [16] for specified values of vapor gas temperature (T_g) and vapor mass fraction (ω_∞). The partial pressure of vapor at the interface ($p_{sat}(T_i)$), is obtained using ALLPROPS [17] as a function of interface temperature. The gas and liquid phase properties used are given in Table 1. The other inputs required to solve the above set of equations are mass transfer coefficient (κ^*), heat transfer coefficient (h_g^*) and mass diffusivity D_{v-nc}.

The values of h_g^* and κ^* are taken from Bird et al. [15] viz.

$$h_g^* = -(\Gamma C_P/a_i)/[\exp(-\Gamma C_P/a_i h_g) - 1] \tag{11}$$

$$\kappa^* = -(\Gamma/a_i)/[\exp(-\Gamma/a_i\kappa) - 1] \tag{12}$$

The vapor side mass transfer coefficient (κ) in Eq. (12) is expressed as a function of the Sherwood number and similarly the vapor side heat transfer coefficient (h_g) in Eq. (11) is obtained as function of Raleigh number. The correlation used for heat transfer coefficient [18] is given below:

$$Nu = \frac{h_g l}{k} = 0.27 Ra^{0.25} \tag{13}$$

The above equation is valid for range of Raleigh numbers from 3×10^5 to 3×10^{10}. For mass transfer coefficient, the Nusselt number and Prandtl number are replaced by Sherwood and Schmidt number, respectively, following Eckert et al. [19] to give

$$Sh = \frac{\kappa_g}{\rho D_{v-nc}} = 0.27\left(Ra\frac{Sc}{Pr}\right)^{0.25} \tag{14}$$

These coefficients (h_g and κ) are used with Eqs. (11) and (12) to determine the heat and mass transfer coefficients in the presence of mass transfer (h_g^* and κ^*).

The mass diffusivity (D_{v-nc}) for binary gas mixtures is inversely proportional to the pressure and increases with increasing temperature and is almost independent of composition for a given gas-pair. The following equation from Bird et al. [15] is used for estimation of D_{v-nc}.

Table 1
Typical properties of cryogenic fluids used in the model

Fluid	Density (kg m^{-3})	Specific heat at constant pressure (kJ kg^{-1} K^{-1})	Viscosity (mPa s)	Thermal conductivity (mW m^{-1} K^{-1})	Latent heat of vaporization (kJ kg^{-1})
LN_2 at 0.20 MPa	778.5	2.080	125.8	131.4	190.9
GN_2 at 100 K	3.484	1.067	6.98	9.33	
GHe at 100 K	0.487	5.2	9.47	73.3	

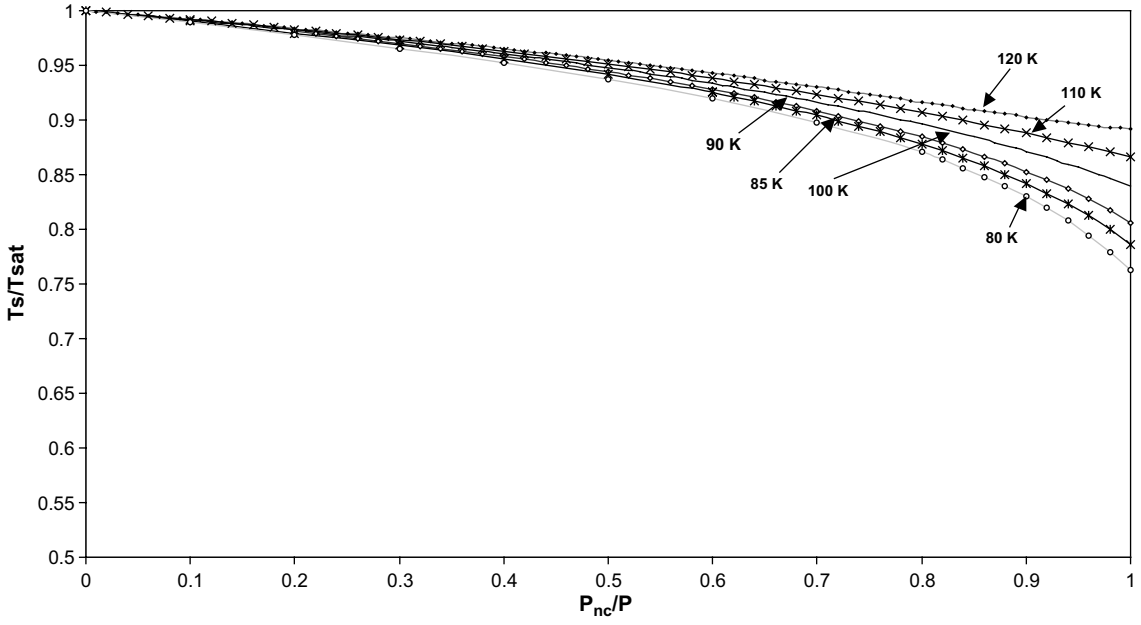

Fig. 12. Predicted variation of surface temperature due to non-condensable gas.

$$\frac{pD_{\mathrm{v-nc}}}{(p_{\mathrm{cv}}p_{\mathrm{cnc}})1/3(T_{\mathrm{cv}}T_{\mathrm{cnc}})5/12\left(\frac{1}{M_{\mathrm{v}}}+\frac{1}{M_{\mathrm{nc}}}\right)^{0.5}} = a\left(\frac{T}{\sqrt{T_{\mathrm{cv}}T_{\mathrm{cnc}}}}\right)^{b} \tag{15}$$

In the above equation, the units of $D_{\mathrm{v-nc}}$ is $\mathrm{cm^2\,s^{-1}}$, p in atmosphere, and T is in K. Constants a and b in Eq. (12) are given by [15]:

$a = 2.745 \times 10^{-4}$,
$b = 1.823$.

The predictions for a stratified layer of LN_2 maintained at a temperature of 79.5 K with the vapor mixture at a pressure of 0.2 MPa and at temperatures between 80 and 120 K are shown in Fig. 12. Various mass fractions of non-condensable helium between 0 and 1 are considered. The interface temperature is plotted as a fraction of the saturation temperature corresponding to total pressure whereas the fraction of non-condensable gas is represented as the ratio of the partial pressure of non-condensable gases to the total pressure. It is seen that as the partial pressure of the non-condensable gas in the ullage increases, the surface temperature decreases. The following two limits of interface temperatures are obtained corresponding to (a) no non-condensable gas being present, i.e., $p_{\mathrm{nc}}/P = 0$, $T_{\mathrm{s}}/T_{\mathrm{sat}}(P) = 1$ and (b) when only non-condensable gas is present, i.e., $p_{\mathrm{nc}}/P = 1.0$. In case of the latter $T_{\mathrm{s}}/T_{\mathrm{sat}}(P)$ varies between 0.89 and 0.76 depending on the temperature of gas with the higher value for a gas temperature of 120 K and the lower value for the gas temperature of 80 K. The predicted values of the surface temperature non-dimensionalized by the saturation temperature are compared with the experimental measurements and the correlation given by Eq. (1) in Fig. 13. The agreement is observed to be reasonable.

5. Conclusions

Experiments carried out with stratified liquid columns of LN_2 stored and depleted from large containers show non-condensable helium gas to reduce the values of interface temperature much below the saturation temperatures corresponding to the total ullage gas pressure. The interface temperature decreases as the concentration of the non-condensable gases is increased. A correlation is obtained for the variations in surface temperature when the ullage gas temperature is not very different from the temperature of the stratified column of liquid. The measurements of the interface temperature are correlated with a diffusion model in which a stratified column of liquid is present. The interface vapor pressure conditions are also determined and correlated with the ullage gas pressure.

A chilled surface layer whose temperature is lower than the stratified column of the stored liquid or the bulk temperature of the liquid is seen to be formed when the liquid is discharged from the container by pressurizing it using a non-condensable gas. The chilled layer is shown to propagate at speeds more than an order of magnitude higher than the characteristic wave speed due to thermal diffusion. The formation of a chilled layer results in the bulk liquid being superheated and could lead to disruptive evaporation and instabilities.

Interface temperature measurements show irregularities and differences from the ullage gas temperature and saturation temperature when the ullage gas pressure is less than the saturation pressure of the liquid referred to the bulk temperature by a factor of about 0.8. Under these

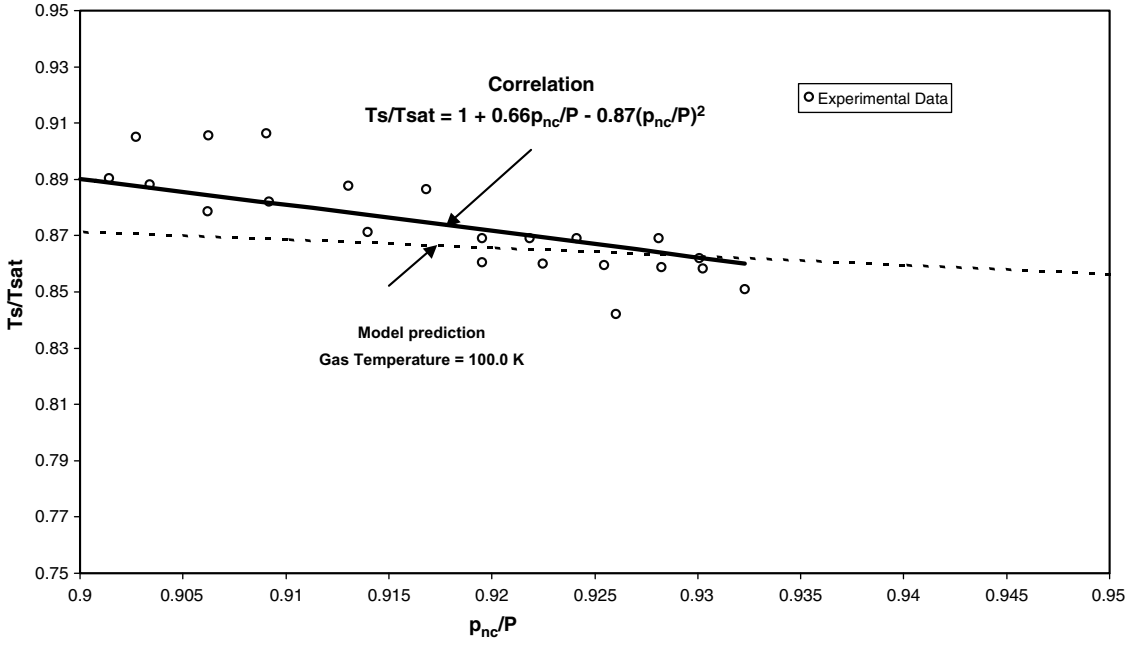

Fig. 13. Comparison of experimental data with prediction.

conditions, the convective transport of the bulk fluid to the surface and a fast evaporation with the entrainment of liquid droplets in the evaporation process is observed.

References

[1] A.P. Kryukov, V.Yu. Levashov, S.S. Sazhin, Evaporation of diesel fuel droplets: kinetic versus hydrodynamic models, Int. J. Heat Mass Transfer 47 (2004) 2541–2549.

[2] A.V. Kozyrev, A.G. Sitnikov, Evaporation of a spherical droplet in a moderate pressure gas, Phys. Usp. 44 (2001) 725–733.

[3] Ralph Scurlock, Low loss dewars and tanks: (4) liquid evaporation mechanisms and instabilities, Coldfacts (2001) 7–18.

[4] F.M. Gerner, C.L. Tien, Axisymmetric interfacial condensation model, J. Heat Transfer 111 (1989) 503–509.

[5] R. Krahl, M. Adamo, A model for two phase flow with evaporation, IISN 0946-8633, 899, Weierstrass-Institut for Angewandte Analysis and Stochastic, Berlin, 2004.

[6] K. Morita, K. Fukuda, Y. Tobita, Sa. Kondo, T. Suzuki, W. Maschek, Generalized modeling of multi-component vaporization/condensation phenomena for multiphase-flow analysis, in: Proceedings of the 10th International Conference on Nuclear Engineering, ICONE10-22229, Arlington, VA, 2002.

[7] G. Moggin, C. Colin, J. Magnaudet, B. Vieille, Transfer through the gas–liquid interface and at the walls of a cryogenic propellant tank, in space launcher liquid propulsion, in: Proceeding of 4th International Conference on Launcher Technology, CNES, Liege, 2002.

[8] J.A. Clark, Review of pressurization, stratification, and interfacial phenomena, Adv. Cryogenics 10 (1965) 259–283.

[9] V.I. Fedorov, E.A. Luk'yanova, Filling and storage of cryogenic propellant components cooled below boiling point in rocket tanks at atmospheric pressure, Chem. Pet. Eng. 36 (2000) 584–587.

[10] G. Fang, C.A. Ward, Temperature measured close to the interface of an evaporating liquid, Phys. Rev. 59 (1999) 417–428.

[11] C. Beduz, R. Rebiai, R.G. Scurlock, Thermal overfill, and the surface vaporization of cryogenic liquids under storage conditions, Adv. Cryogenics 29 (1984) 795–803.

[12] R.J. Peterson, S.S. Grewal, M.M. El-Wakil, Investigation of liquid flashing and evaporation due to sudden depressurization, Int. J. Heat Mass Transfer 27 (1984) 301–310.

[13] T. Gemci, K. Yakut, N. Chigier, T.C. Ho, Flash atomization of water/acetone solutions, Atomization Sprays 14 (2004) 459–475.

[14] L. Manalo, K.M. Akyuzlu, A study of unsteady natural convection in cryogenic storage tanks for densified propellants, in: Proceedings of IMECE'03, Washington, DC, November 16–21, 2003.

[15] B. Bird, W.E. Stewart, E.N. Lightfoot, Transport Phenomena, John Wiley and Sons, New York, 1960.

[16] R.L. Burden, J.D. Faires, A. Reynolds, Numerical Analysis, Weber and Schmidt, Boston, Massachusetts, 1978, pp. 443–450.

[17] ALLPROPS, Center for applied thermodynamic studies, University of Idaho.

[18] W.H. McAdams, Heat Transmission, third ed., McGraw-Hill, New York, 1964.

[19] E.R.G. Eckert, R.M. Drake Jr., Analysis of Heat and Mass Transfer, Hemispheric Publishing Corporation, 1987, pp. 731–732.